To be published in Applied Optics:

Title:	Analysis of Experimental Errors in Mueller Matrix Channeled Polarimeters
Authors:	Luis Gonzalez-Siu,Neil Bruce
Accepted:	15 May 21
Posted	18 May 21
DOI:	https://doi.org/10.1364/AO.430923

Analysis of Experimental Errors in Mueller Matrix Channeled Polarimeters

LUIS OSCAR GONZÁLEZ-SIU[1,*] AND NEIL C. BRUCE[1,2]

[1] Instituto de Ciencias Aplicadas y Tecnología, Universidad Nacional Autónoma de México, Circuito Exterior S/N, Ciudad Universitaria, 04510, Mexico City
[2] neil.bruce@icat.unam.mx
[*] Corresponding author: oscargsiu@gmail.com

Compiled May 18, 2021

In this work we analyse the effect of experimental errors and measurement noise on Mueller matrix channeled spectropolarimeters. The main advantage of this type of polarimeter is the independence on temporal resolution, as it can be used as a snapshot polarimeter. The simulation of the polarimeters with experimental errors and two published extraction methods of the sample Mueller matrix are also presented. The Mueller matrix Channeled Spectropolarimeter (MMCS) setup is composed of a mirrored Stokes Channeled Spectropolarimeter (SCS) as the polarization states generator (PSG) and a SCS as the polarization states analyzer (PSA). The SCS setup is composed of two thick birefringent retarders followed by a horizontal linear polarizer. The effects of the thickness' ratio of the retarders, the global retardance factor, retardance errors, axes alignment errors, and additive Gaussian noise are studied to optimize the MMCS setups. In this work we do not include a calibration procedure to improve the measured Mueller matrix parameters, but we study the sensitivity of the polarimeter to the different configurations and error sources.

http://dx.doi.org/10.1364/ao.XX.XXXXXX

1. INTRODUCTION

Mueller matrix polarimeters measure the full or partial Mueller matrix of a sample or optical component. One of the difficulties of traditional polarimetric measurements is the requirement for quasi-monochromatic illumination, or a single measurement position, to be able to have a fast and simple measurement procedure. Channeled polarimeters (CP) with spatial or spectral channeling have been developed to overcome this type of limitation, and to permit snapshot polarimetry [1, 2]. In particular the spectroscopic analysis of the state of polarization (SOP) of light plays a major role in polarimetric and ellipsometric studies of dispersive materials [3, 4]. Spectropolarimetry has been widely applied in various application fields, such as remote sensing [5, 6], material characterization [7, 8], and synthesis of novel materials [9–11].

In this paper, we study the sensitivity of the measured Mueller matrix by a Mueller matrix Channeled Spectropolarimeter (MMCS) to possible configurations and experimental errors. We study the effects of the thickness' ratio of the polarimeter retarders, the global retardance factor, retardance errors, axes alignment errors, and additive Gaussian noise, extending a previous study on the effect of these errors on a Stokes Channeled Spectropolarimeter (SCS) [12]. In this work we do not include a calibration procedure to improve the measured Mueller matrix parameters, but we study the sensitivity of the polarimeter to the error sources. In Section 2 we present two published methods to extract the Mueller matrix of the sample. In Section 3 we present the results of various simulations of different configurations and error sources. The paper ends with some concluding remarks in Section 4.

2. CHANNELED SPECTROPOLARIMETRY

Mueller matrix channeled polarimetry has been analyzed as a snapshot technique to measure spectral or spatial polarization characteristics [2]. Temporal misregistration, or intensity differences between time-sequential measurements not induced by polarization, can be a significant source of error in certain applications. Such misregistration can be caused by motion of the polarimeter or the sample [13, 14].

CP techniques make use of polarization interference in order to amplitude modulate the Mueller matrix components onto either spectral or spatial carrier frequencies. CP enables the direct measurement of all sixteen Mueller matrix components simultaneously, by performing the addition and subtraction optically [2].

Interference of the different polarization components of the beam maintains the phase of each component within the complex amplitude, before the detector measures the intensity. Consequently, the amplitude and phase of the Mueller matrix elements are encoded within the amplitude and phase of the carrier

frequency, enabling the magnitude and sign (or handedness) of the components to be extracted [14].

As CP is a snapshot method, there are no problems of image registration between the intensity measurements [14, 15]. This avoids the creation of false polarization signatures which can occur in the spectrum or scene. Since a given Mueller parameter is calculated interferometrically and measured directly, image registration between several intensity measurements is unnecessary. Furthermore, since each parameter is modulated on coincident carrier frequencies, spatial or spectral registration between all the parameters is inherent. This significantly reduces the complexity of the Mueller matrix calculation over conventional polarimeters. However, these benefits come at a tradeoff, typically to the spatial and spectral resolution of the sensor [14]. This type of cosinusoidally modulated spectrum is widely used in the field of frequency-domain interferometry and is called a channeled spectrum [4].

The MMCS setup studied (see Fig. 1) is composed of a SCS as the PSA, whereas the PSG is a mirror image of the PSA. The SCS setup is composed of two thick birefringent retarders ($\underline{\underline{\mathbf{M}}}_R$) followed by a horizontal linear polarizer ($\underline{\underline{\mathbf{M}}}_P$) [16–18]. Then, the MMCS setup is given by

$$\begin{aligned}\underline{\underline{\mathbf{W}}} =& \underline{\underline{\mathbf{M}}}_{P2}(0)\underline{\underline{\mathbf{M}}}_{R4}(\phi_4,\pi/2)\underline{\underline{\mathbf{M}}}_{R3}(\phi_3,0)\underline{\underline{\mathbf{M}}}\times \\ &\times \underline{\underline{\mathbf{M}}}_{R2}(\phi_2,0)\underline{\underline{\mathbf{M}}}_{R1}(\phi_1,\pi/2)\underline{\underline{\mathbf{M}}}_{P1}(0),\end{aligned} \tag{1}$$

where $\underline{\underline{\mathbf{M}}}$ is the Mueller matrix of the sample. The retarders $\underline{\underline{\mathbf{M}}}_{R2}, \underline{\underline{\mathbf{M}}}_{R3}$ are aligned at 0°, the retarders $\underline{\underline{\mathbf{M}}}_{R1}, \underline{\underline{\mathbf{M}}}_{R4}$ at 45°, and the polarizers $\underline{\underline{\mathbf{M}}}_{P1}, \underline{\underline{\mathbf{M}}}_{P2}$ at 0°. The corresponding Mueller matrices are given by

$$\underline{\underline{\mathbf{M}}}_{Pj}(0) = \frac{1}{2}\begin{pmatrix}1&1&0&0\\1&1&0&0\\0&0&0&0\\0&0&0&0\end{pmatrix}, j=1,2, \tag{2}$$

$$\underline{\underline{\mathbf{M}}}_{Rj}(\phi_j,0) = \begin{pmatrix}1&0&0&0\\0&1&0&0\\0&0&cos\phi_j&sin\phi_j\\0&0&-sin\phi_j&cos\phi_j\end{pmatrix}, j=2,3, \tag{3}$$

$$\underline{\underline{\mathbf{M}}}_{Rj}(\phi_j,\pi/2) = \begin{pmatrix}1&0&0&0\\0&cos\phi_j&0&-sin\phi_j\\0&0&1&0\\0&sin\phi_j&0&cos\phi_j\end{pmatrix}, j=1,4, \tag{4}$$

where ϕ_j is the retardance of the thick birefringent retarders given by $\phi_j = 2\pi\sigma\tau_j$ with $\tau_j = d_0 d_j B$; σ, the wavenumber; τ_i, the optical path difference (OPD); d_0, the global retardance factor in mm; d_j, the local retardance factor; and B, the birefringence of the retarder. The product $d_0 d_i$ is the retarder's thickness.

For this setup, an unpolarized light source with intensity $I_0(\sigma)$ and a polarization-insensitive detector are considered. The irradiance measured by the detector is given by

$$I(\sigma) = \begin{pmatrix}1&0&0&0\end{pmatrix}\underline{\underline{\mathbf{W}}}\begin{pmatrix}I_0&0&0&0\end{pmatrix}^T. \tag{5}$$

Substituting the system matrix given by Eq. (1) and developing Eq. (5) yields

$$I(\sigma) = \frac{1}{4}I_0(\sigma)X(\sigma), \tag{6}$$

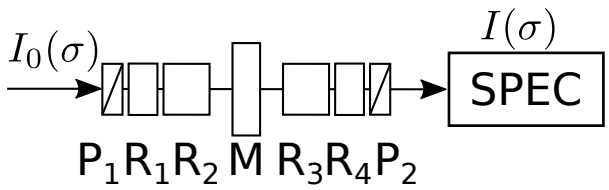

Fig. 1. Mueller matrix channeled spectropolarimeter setup composed of a SCS as the PSA and a mirrored SCS as the PSG.

where

$$X(\sigma) = \begin{pmatrix}1 & C\phi_4 & S\phi_3 S\phi_4 & -C\phi_3 S\phi_4\end{pmatrix}\underline{\underline{\mathbf{M}}}\begin{pmatrix}1\\C\phi_1\\S\phi_1 S\phi_2\\S\phi_1 C\phi_2\end{pmatrix}, \tag{7}$$

and $C\phi_j = \cos(\phi_j)$ and $S\phi_j = \sin(\phi_j)$. Therefore, the expected modulations of the MMCS are given by

$$\begin{aligned}X(\sigma) =& \\ &+ m_{00} && + m_{01}C\phi_1 \\ &+ m_{02}S\phi_1 S\phi_2 && + m_{03}S\phi_1 C\phi_2 \\ &+ m_{10}C\phi_4 && + m_{11}C\phi_1 C\phi_4 \\ &+ m_{12}S\phi_1 S\phi_2 C\phi_4 && + m_{13}S\phi_1 C\phi_2 C\phi_4 \\ &+ m_{20}S\phi_3 S\phi_4 && + m_{21}C\phi_1 S\phi_3 S\phi_4 \\ &+ m_{22}S\phi_1 S\phi_2 S\phi_3 S\phi_4 && + m_{23}S\phi_1 C\phi_2 S\phi_3 S\phi_4 \\ &- m_{30}C\phi_3 S\phi_4 && - m_{31}C\phi_1 C\phi_3 S\phi_4 \\ &- m_{32}S\phi_1 S\phi_2 C\phi_3 S\phi_4 && - m_{33}S\phi_1 C\phi_2 C\phi_3 S\phi_4.\end{aligned} \tag{8}$$

It is observed that the MMCS works with up to 49 channels (including a central channel C_0 and 24 negative channels, see Table 1), and that the spectrometer resolution must be sufficient to resolve all these channels [19].

For the Mueller matrix components extraction, we studied two methods: (1) the Measurement matrix method [20], which we use only as a reference method and to characterize the polarimeters, and (2) the Analytical Channel Splitting method proposed by Alenin and Tyo [1, 2]. A Channel Splitting method, similar to one proposed by Oka and Kato for SCS systems [4], was developed by Hagen, Oka, and Dereniak [21] for a specific MMCS configuration, but is out of the scope of this paper.

A. Measurement matrix method

A series of analyzing polarization states (vectors) and generating vectors are predetermined

$$\underline{\mathbf{A}}_n = \begin{pmatrix}a_0 & a_1 & a_2 & a_3\end{pmatrix}_n^T, \tag{9}$$

$$\underline{\mathbf{G}}_n = \begin{pmatrix}g_0 & g_1 & g_2 & g_3\end{pmatrix}_n^T, \tag{10}$$

so the irradiance measured is given by

$$I(\sigma_n) = \underline{\mathbf{A}}_n^T\,\underline{\underline{\mathbf{M}}}\,\underline{\mathbf{G}}_n, \tag{11}$$

which can be shown is equivalent to

$$I(\sigma_n) = \underline{\mathbf{D}'}_n^T\,\underline{\mathbf{M}}', \tag{12}$$

where $\underline{\mathbf{D}}'_n$ is the dyad product $\underline{\underline{\mathbf{D}}}_n = \underline{\mathbf{A}}_n \underline{\mathbf{G}}_n^T$ reshaped into a vector

$$\underline{\mathbf{D}}'_n = \underline{\mathbf{A}}_n \otimes \underline{\mathbf{G}}_n \tag{13}$$

$$= \begin{pmatrix} a_0 g_0 & \dots & a_0 g_3 & \dots & a_3 g_0 & \dots & a_3 g_3 \end{pmatrix}_n^T, \tag{14}$$

and $\underline{\mathbf{M}}'$ is the Mueller matrix reshaped into a Mueller vector [2]

$$\underline{\mathbf{M}}' = (m_{00}\, m_{01}\, m_{02}\, m_{03} \dots m_{30}\, m_{31}\, m_{32}\, m_{33})^T. \tag{15}$$

Developing and rearranging Eq. (12) yields

$$\underline{\mathbf{I}} = \underline{\underline{\mathbf{W}}}' \underline{\mathbf{M}}', \tag{16}$$

where

$$\underline{\underline{\mathbf{W}}}' = \begin{pmatrix} \underline{\mathbf{D}}'_0 & \underline{\mathbf{D}}'_1 & \dots & \underline{\mathbf{D}}'_{N-1} \end{pmatrix}^T. \tag{17}$$

Therefore, $\underline{\underline{\mathbf{W}}}'$ is a matrix containing the states of analysis-generation defined by the combination of the PSA and PSG of the MMCS [1, 2].

The extraction of the Mueller matrix elements is achieved by inverting the process:

$$\underline{\mathbf{M}}' = \underline{\underline{\mathbf{W}}}'^{+} \underline{\mathbf{I}}, \tag{18}$$

where $\underline{\underline{\mathbf{W}}}'^{+}$ is the pseudo-invere of $\underline{\underline{\mathbf{W}}}'$. However, this method considers the $\underline{\underline{\mathbf{M}}}$-matrix invariant with wavenumber, therefore, it is used only as a reference.

B. Analytical Channel Splitting method

The inverse Fourier transform of $I(\sigma)$ [Eq. (6)] gives the autocorrelation function $C(\tau)$ [4], which describes the modulation channels in the τ-domain (OPD-space) of the spectrum of the Mueller matrix components we want to know. The Fourier transforms of the modulations present in Eq. (8) are

$$1(\sigma) \longleftrightarrow \delta(\tau), \tag{19}$$

$$\cos(2\pi\sigma\tau_j) \longleftrightarrow \frac{1}{2}[\delta(\tau+\tau_j) + \delta(\tau-\tau_j)], \tag{20}$$

$$\sin(2\pi\sigma\tau_j) \longleftrightarrow \frac{J}{2}[\delta(\tau+\tau_j) - \delta(\tau-\tau_j)], \tag{21}$$

where δ, with no subscript, is the Dirac delta function, and τ is the Fourier transform variable of σ [1, 2, 14].

A construct is needed to recreate the modulations in the Fourier domain in an analytical form. This is obtained through a Frequency Phase Matrix (FPM), which determines the functional form of the modulation and makes Fourier transforms a matter of looking up the correct row of a precalculated matrix [1, 2]. Using the FPM, we obtain a map for each Mueller element splitting called the $\underline{\underline{\mathbf{Q}}}$-matrix [1], which maps the vectorized Mueller matrix into a channel vector $\underline{\mathbf{C}}$

$$\underline{\mathbf{C}} = \underline{\underline{\mathbf{Q}}} \mathcal{F}^{-1}\{\underline{\mathbf{M}}'\}, \tag{22}$$

where $\underline{\mathbf{C}}$ is a matrix formed by concatenating the filtered channels of the autocorrelation function $C(\tau) = \mathcal{F}^{-1}\{I(\sigma)\}$ [2].

From the setup of interest (see Fig. 1), all θ's are steps of 45°, which collapses $\cos(2\theta)$ and $\sin(2\theta)$ to either ± 1 or 0. As a result, only retardance contributes to the modulation [1]. We propose a template (see Table 1) for the $\underline{\underline{\mathbf{Q}}}$-matrix based on the local retardance factors. We construct the $\underline{\underline{\mathbf{Q}}}$-matrix by rearranging the rows of the template following the relative positions of the channels, given by comparison of the local retardance factors.

The $\underline{\underline{\mathbf{Q}}}$-matrix has a cardinality $[N_C \times M]$ where $M = 16$ and N_C is the number of channels or modulations, given by [1, 2]

$$N_C = 1 + 2\sum_{j=1}^{4} d_j. \tag{23}$$

To extract the sample Mueller matrix an inverse map is required, which is a matrix that determines which channels have to be combined in order to extract the Mueller matrix components [1]. That inverse map corresponds to the pseudo-inverse $\underline{\underline{\mathbf{Q}}}^{+}$,

$$\underline{\mathbf{M}}' = \underline{\underline{\mathbf{Q}}}^{+} \mathcal{F}\{\underline{\mathbf{C}}\}. \tag{24}$$

This method corresponds to the Generalized Channeled Polarimetry methodology proposed by Alenin and Tyo [2].

It is important to note that a phase shift must be corrected when applying the Fourier transform to the filtered channels. For this, we analyse each possible channel and multiply it by a phase cancellation term corresponding to the retardance ϕ_j to each channel $C_j(\tau)$. This approach is mostly helpful for cases with crosstalk between channels (e.g., $\tau_1 - \tau_2 = \tau_2$).

3. SIMULATIONS, RESULTS, AND DISCUSSION OF MMCS CONFIGURATIONS

The general methodology for the MMCS simulations is as follows:

1. Select a sample (a Mueller matrix).
2. Define the MMCS configuration, including the spectral range $[\sigma_{min}, \sigma_{max}]$, the spectral resolution $\Delta\sigma$, the number of pixels N in the irradiance spectrum, the nominal global retardance factor, the nominal local retardance factors (thickness ratio), and the sources of error (retardance errors Δd_j, alignment errors ϵ_j, and Gaussian noise amplitude).
3. Run the methods reviewed to simulate the irradiance to be measured.
4. Run the inverse methods to extract the sample's Mueller matrix from the irradiance measured, for this purpose consider the irradiance obtained with Eq. (5) with no experimental errors.

The MMCS consists of a mirrored SCS (PSG) followed by the sample and a SCS (PSA), as discussed before (see Fig. 1). The transmission axis of the horizontal linear polarizer in the PSG is the system's reference (0°). For the spectrometer, a σ-wavenumber range from 1.4954×10^4 cm^{-1} to 1.8408×10^4 cm^{-1}] (λ from 543 to 668 nm), with a sampling number N of 2048 pixels, and a corresponding wavenumber resolution of $(\sigma_{max} - \sigma_{min})/N$ were considered. In the simulation, the system was illuminated with an unpolarized light source with a varying spectral intensity. The high-order retarders were assumed to be made of quartz, and the birefringence was calculated using a model proposed by Ghosh [22]. The retardance shift for the retarders is between 84.68 and 106.10 rad/mm for the wavenumber range. The sample selected for the results reported is air (considered invariant with wavelength).

Reconstruction artifacts, associated with the Fast Fourier Transform (FFT) method applied, appear when extracting the Mueller matrix. This is a well-known effect, due to a lack of periodicity in the irradiance measured, contradicting the FFT

Table 1. MMCS Q-matrix template.

Index	OPD	m_{00}	m_{01}	m_{02}	m_{03}	m_{10}	m_{11}	m_{12}	m_{13}	m_{20}	m_{21}	m_{22}	m_{23}	m_{30}	m_{31}	m_{32}	m_{33}	Factor
24	$+\tau_1-\tau_2-\tau_3-\tau_4$											-1	$+\jmath$			$-\jmath$	-1	1/16
23	$+\tau_1-\tau_2-\tau_3+\tau_4$											$+1$	$-\jmath$			$+\jmath$	$+1$	1/16
22	$+\tau_1-\tau_2+\tau_3-\tau_4$											$+1$	$-\jmath$			$-\jmath$	-1	1/16
21	$+\tau_1-\tau_2+\tau_3+\tau_4$											-1	$+\jmath$			$+\jmath$	$+1$	1/16
20	$+\tau_1+\tau_2-\tau_3-\tau_4$											$+1$	$+\jmath$			$+\jmath$	-1	1/16
19	$+\tau_1+\tau_2-\tau_3+\tau_4$											-1	$-\jmath$			$-\jmath$	$+1$	1/16
18	$+\tau_1+\tau_2+\tau_3-\tau_4$											-1	$-\jmath$			$+\jmath$	-1	1/16
17	$+\tau_1+\tau_2+\tau_3+\tau_4$											$+1$	$+\jmath$			$-\jmath$	$+1$	1/16
16	$+\tau_1-\tau_3-\tau_4$										-1				$-\jmath$			1/8
15	$+\tau_1-\tau_3+\tau_4$										$+1$				$+\jmath$			1/8
14	$+\tau_1+\tau_3-\tau_4$										$+1$				$-\jmath$			1/8
13	$+\tau_1+\tau_3+\tau_4$										-1				$+\jmath$			1/8
12	$+\tau_1-\tau_2-\tau_4$							$+1$	$-\jmath$									1/8
11	$+\tau_1-\tau_2+\tau_4$							$+1$	$-\jmath$									1/8
10	$+\tau_1+\tau_2-\tau_4$							-1	$-\jmath$									1/8
9	$+\tau_1+\tau_2+\tau_4$							-1	$-\jmath$									1/8
8	$+\tau_3-\tau_4$									$+1$				$-\jmath$				1/4
7	$+\tau_3+\tau_4$									-1				$+\jmath$				1/4
6	$+\tau_1-\tau_4$						$+1$											1/4
5	$+\tau_1+\tau_4$						$+1$											1/4
4	$+\tau_1-\tau_2$			$+1$	$-\jmath$													1/4
3	$+\tau_1+\tau_2$			-1	$-\jmath$													1/4
2	$+\tau_4$					$+1$												1/2
1	$+\tau_1$		$+1$															1/2
0	0	$+1$																1
-1	$-\tau_1$		$+1$															1/2
-2	$-\tau_4$					$+1$												1/2
-3	$-\tau_1-\tau_2$			-1	$+\jmath$													1/4
-4	$-\tau_1+\tau_2$			$+1$	$+\jmath$													1/4
-5	$-\tau_1-\tau_4$						$+1$											1/4
-6	$-\tau_1+\tau_4$						$+1$											1/4
-7	$-\tau_3-\tau_4$									-1				$-\jmath$				1/4
-8	$-\tau_3+\tau_4$									$+1$				$+\jmath$				1/4
-9	$-\tau_1-\tau_2-\tau_4$							-1	$+\jmath$									1/8
-10	$-\tau_1-\tau_2+\tau_4$							-1	$+\jmath$									1/8
-11	$-\tau_1+\tau_2-\tau_4$							$+1$	$+\jmath$									1/8
-12	$-\tau_1+\tau_2+\tau_4$							$+1$	$+\jmath$									1/8
-13	$-\tau_1-\tau_3-\tau_4$										-1				$-\jmath$			1/8
-14	$-\tau_1-\tau_3+\tau_4$										$+1$				$+\jmath$			1/8
-15	$-\tau_1+\tau_3-\tau_4$										$+1$				$-\jmath$			1/8
-16	$-\tau_1+\tau_3+\tau_4$										-1				$+\jmath$			1/8
-17	$-\tau_1-\tau_2-\tau_3-\tau_4$											$+1$	$-\jmath$			$+\jmath$	$+1$	1/16
-18	$-\tau_1-\tau_2-\tau_3+\tau_4$											-1	$+\jmath$			$-\jmath$	-1	1/16
-19	$-\tau_1-\tau_2+\tau_3-\tau_4$											-1	$+\jmath$			$+\jmath$	$+1$	1/16
-20	$-\tau_1-\tau_2+\tau_3+\tau_4$											$+1$	$-\jmath$			$-\jmath$	-1	1/16
-21	$-\tau_1+\tau_2-\tau_3-\tau_4$											-1	$-\jmath$			$-\jmath$	$+1$	1/16
-22	$-\tau_1+\tau_2-\tau_3+\tau_4$											$+1$	$+\jmath$			$+\jmath$	-1	1/16
-23	$-\tau_1+\tau_2+\tau_3-\tau_4$											$+1$	$+\jmath$			$-\jmath$	$+1$	1/16
-24	$-\tau_1+\tau_2+\tau_3+\tau_4$											-1	$-\jmath$			$+\jmath$	-1	1/16

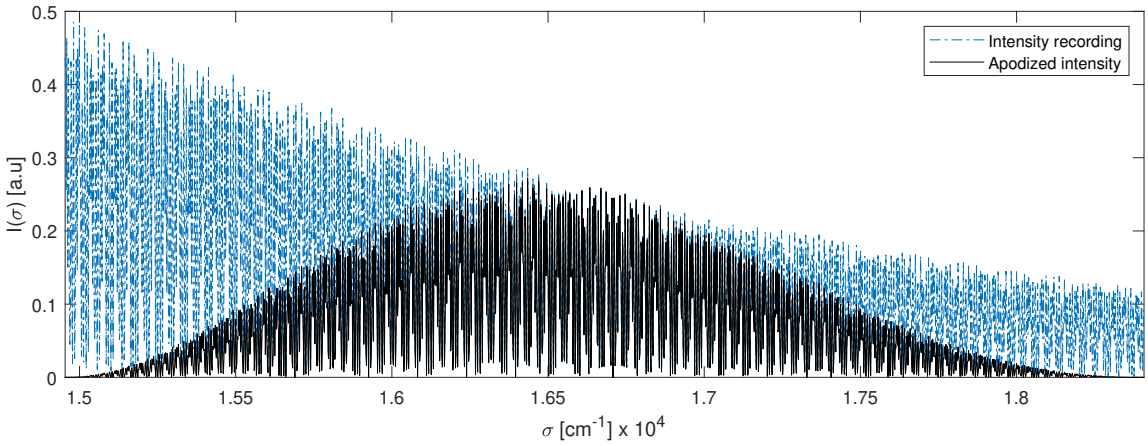

Fig. 2. Intensity recording (dashed light blue line) and apodized intensity (solid black line) using a configuration $(1, 2, 5, 10)$, a global retardance factor $d_0 = 10$ mm, and an unpolarized light source with a varying spectral intensity, for the simulated air sample with SOP invariant with wavenumber.

supposition of a periodic function. Therefore, before computing the FFT, to prevent discontinuities in the periodic continuation, apodization has to be applied to the raw data (see Fig. 2) [11, 23, 24]. In this work, a Hann window was applied [25],

$$\omega = \frac{1}{2}\left(1 - \cos\frac{2\pi n}{N}\right),\ n = 0, 1, 2, ..., N-1. \tag{25}$$

However this step may aggravate the discrepancies at the edges of the spectrum, where the division is nearly by zero [23].

To evaluate the performance of the MMCS setups of interest, three figures of merit were considered: (1) the root mean square error (RMS) of the extracted elements m_{ij} against their corresponding nominal values $m_{ij,nom}$, given by

$$\mathrm{RMS}(m_{ij}) = \left[N^{-1}\sum_{n=1}^{N}(m_{ij} - m_{ij,nom})_n^2\right]^{1/2}, \tag{26}$$

(2) the condition number (CN) of the $\underline{\underline{\mathbf{W}}}$-Mueller matrix and the $\underline{\underline{\mathbf{Q}}}$-matrix of the nominal setup, and (3) the equally weighted variance (EWV) [26] for the same matrices given by

$$\mathrm{EWV}(\underline{\underline{\mathbf{A}}}) = \mathrm{Tr}[(\underline{\underline{\mathbf{A}}}^{+})^T\underline{\underline{\mathbf{A}}}^{+}], \tag{27}$$

where $\underline{\underline{\mathbf{A}}}^{+}$ is the pseudo-inverse of $\underline{\underline{\mathbf{A}}}$. These metrics are used to evaluate the noise immunity of the MMCS setups [27]. For this work, an extracted parameter is considered immune when RMS values are < 0.01. To avoid the discrepancies at the edges of the spectra, a consequence of apodization [23], the RMS was calculated for a reduced wavenumber range from 1.5×10^4 cm^{-1} to 1.83×10^4 cm^{-1}.

A. Thickness' ratio

Six retarder thickness' ratios were considered: (1,2,3,5), (1,2,4,8), (1,2,5,10), (1,4,2,9), (2,1,4,11), and (2,1,5,12), with a global retardance factor $d_0 = 10$ mm. Figure 3 shows the corresponding autocorrelation function $|C(\tau)|$ for these thickness' ratios. Figure 4 shows the EWV and CN plots for the thickness' ratios of interest. The normalized Mueller matrix elements (m_{ij}/m_{00}) for air are shown in Fig. 5, and the RMS values for the extracted Mueller matrix $\underline{\underline{\mathbf{M}}}$ and its elements m_{ij} are shown in Table 2. The configurations $(1, 4, 2, 9)$, $(2, 1, 4, 11)$, and $(2, 1, 5, 12)$ have the lowest EWV and CN values, and the last two along with the configuration $(1, 2, 5, 10)$ have the smallest total RMS values.

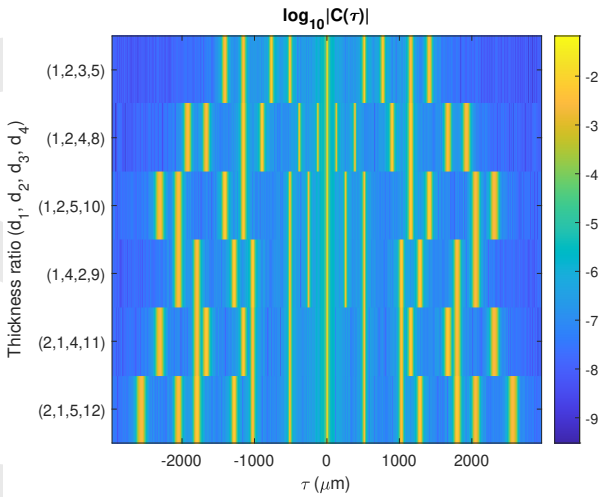

Fig. 3. Autocorrelation function $|C(\tau)|$ for the MMCS with different thickness' ratios and a global retardance factor $d_0 = 10$ mm.

B. Global retardance factor

The MMCS configuration $(1, 2, 5, 10)$ was used from this test forward, as it has been studied before [1, 21]. Inspired by the dual-rotating-retarder Mueller matrix polarimeter [28], Hagen *et al.* chose a $5:1$ ratio of thickness for the pair of analysing retarders to the generating pair to give a compact result. Furthermore, Hagen *et al.* selected a $2:1$ ratio of thicknesses for the retarders within each pair giving a set of thicknesses designated as a $(1, 2, 5, 10)$ configuration [21].

The extracted Mueller matrix using a global retardance factor d_0 from 1 to 15 mm is shown in Fig. 6. From the RMS values (see Table 3), it is observed that the MMCS performance generally improves when the global retardance factor is increased. Furthermore, the lowest total RMS is obtained with $d_0 = 15$ mm, and a total RMS error < 0.01 is achieved for $d_0 \geq 4$ mm. Considering this condition, the lowest EWV($\underline{\underline{\mathbf{W}}}$) is obtained with $d_0 = 15$ mm and the lowest CN($\underline{\underline{\mathbf{W}}}$), with $d_0 = 4$ mm (see Fig. 7).

Table 2. RMS of extracted Mueller matrix M and its elements m_{ij} (air sample) using different thickness' ratio configurations (d_1, d_2, d_3, d_4).

	(1,2,3,5)	(1,2,4,8)	(1,2,5,10)	(1,4,2,9)	(2,1,4,11)	(2,1,5,12)
$\underline{\underline{\mathbf{M}}}$	3.63E-03	4.46E-03	3.03E-03	3.05E-03	3.02E-03	2.96E-03
m_{00}	7.45E-03	7.47E-03	7.45E-03	7.45E-03	7.45E-03	7.45E-03
m_{01}	1.45E-03	2.30E-03	2.01E-04	1.22E-04	4.32E-05	5.38E-05
m_{02}	3.65E-04	4.42E-03	2.10E-04	1.62E-04	1.18E-04	3.32E-04
m_{03}	1.38E-03	4.84E-03	1.98E-04	2.05E-04	4.37E-04	4.28E-04
m_{10}	1.56E-04	2.87E-04	4.49E-04	2.53E-04	3.05E-05	2.70E-05
m_{11}	1.23E-03	3.09E-03	1.22E-03	1.29E-03	4.73E-03	3.05E-03
m_{12}	9.37E-05	1.16E-04	3.66E-05	9.13E-04	1.85E-03	2.27E-04
m_{13}	3.48E-03	3.65E-03	3.34E-03	2.90E-03	3.59E-03	3.64E-04
m_{20}	8.39E-05	3.48E-04	3.30E-04	1.14E-04	1.17E-04	2.89E-04
m_{21}	5.76E-03	5.08E-03	2.32E-03	3.61E-03	1.99E-03	2.60E-04
m_{22}	8.65E-03	7.85E-03	3.24E-03	5.34E-03	2.95E-03	1.76E-03
m_{23}	2.54E-03	1.95E-03	2.23E-03	3.91E-03	2.97E-03	6.33E-03
m_{30}	5.17E-05	8.45E-05	1.35E-04	3.62E-04	1.02E-04	4.28E-04
m_{31}	2.57E-03	4.82E-03	4.48E-03	3.12E-03	3.44E-03	2.61E-04
m_{32}	2.50E-03	8.42E-03	5.92E-03	3.08E-03	3.02E-03	4.35E-03
m_{33}	3.15E-03	2.50E-03	1.54E-03	2.49E-03	2.99E-03	3.53E-03

Table 3. RMS $\times 10^2$ of extracted Mueller matrix M and its elements m_{ij} (air sample) for the global retardance factor d_0 from 1 to 15 mm.

	Global retardance factor d_0 mm														
	1	2	3	4	5	6	7	8	9	10	11	12	13	14	15
$\underline{\underline{\mathbf{M}}}$	164.87	61.63	32.45	0.52	0.61	0.44	0.37	0.35	0.31	0.31	0.25	0.28	0.30	0.28	0.24
m_{00}	17.78	0.84	0.69	0.73	0.74	0.74	0.74	0.74	0.74	0.75	0.74	0.75	0.75	0.75	0.75
m_{01}	121.31	124.53	2.87	0.69	1.61	0.46	0.23	0.28	0.18	0.05	0.10	0.03	0.02	0.04	0.02
m_{02}	11.88	2.26	1.06	0.34	0.25	0.28	0.03	0.17	0.02	0.07	0.02	0.02	0.02	0.02	0.01
m_{03}	200.97	193.65	0.62	1.36	1.15	0.27	0.39	0.11	0.06	0.04	0.12	0.02	0.02	0.02	0.01
m_{10}	69.45	70.91	35.41	0.14	0.54	0.52	0.14	0.08	0.06	0.07	0.04	0.02	0.04	0.01	0.01
m_{11}	148.66	1.66	0.12	0.15	0.18	0.83	0.23	0.12	0.22	0.40	0.23	0.39	0.12	0.17	0.32
m_{12}	160.35	1.60	0.30	0.14	0.12	0.02	0.03	0.01	0.01	0.02	0.01	0.01	0.00	0.00	0.01
m_{13}	23.93	1.89	0.29	0.41	0.44	0.15	0.37	0.31	0.17	0.18	0.07	0.23	0.33	0.30	0.20
m_{20}	39.39	35.65	17.69	0.07	0.15	0.05	0.12	0.09	0.04	0.08	0.05	0.03	0.03	0.01	0.01
m_{21}	176.65	4.75	35.33	0.24	0.34	0.13	0.29	0.38	0.18	0.27	0.20	0.30	0.23	0.36	0.17
m_{22}	360.05	9.93	70.68	0.35	0.61	0.26	0.51	0.56	0.58	0.54	0.18	0.36	0.32	0.52	0.22
m_{23}	179.68	3.04	35.60	0.43	0.25	0.22	0.22	0.13	0.31	0.30	0.27	0.14	0.22	0.19	0.20
m_{30}	40.73	35.27	17.70	0.10	0.17	0.11	0.19	0.08	0.05	0.02	0.04	0.04	0.01	0.01	0.01
m_{31}	114.11	3.88	35.27	0.24	0.15	0.26	0.45	0.39	0.26	0.21	0.07	0.30	0.45	0.20	0.09
m_{32}	229.42	7.44	70.41	0.83	0.31	0.94	0.68	0.73	0.43	0.45	0.23	0.34	0.59	0.18	0.24
m_{33}	253.23	1.88	35.34	0.29	0.43	0.41	0.39	0.20	0.41	0.32	0.37	0.17	0.15	0.23	0.26

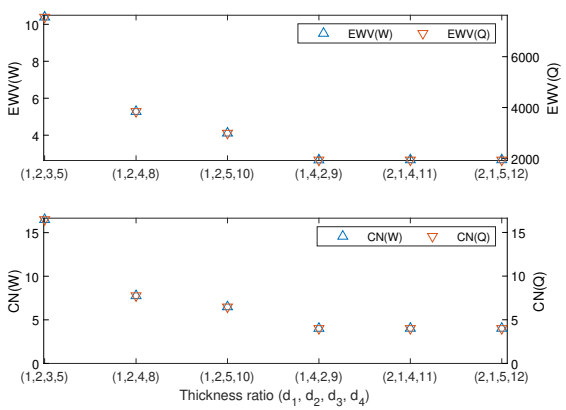

Fig. 4. EWV and CN of the **W**- and **Q**-matrix for the MMCS configurations $(1,2,3,5)$, $(1,2,4,8)$, $(1,2,5,10)$, $(1,4,2,9)$, $(2,1,4,11)$, and $(2,1,5,12)$ and a global retardance factor $d_0 = 10$ mm.

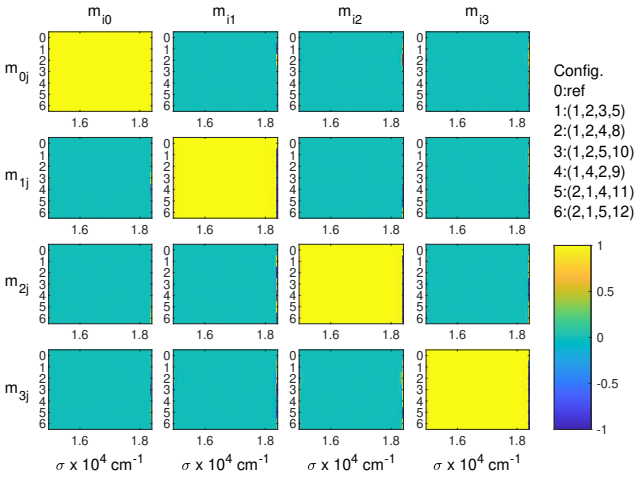

Fig. 5. Normalized Mueller matrix elements (m_{ij}/m_{00}) for the configurations $(1,2,3,5)$, $(1,2,4,8)$, $(1,2,5,10)$, $(1,4,2,9)$, $(2,1,4,11)$, and $(2,1,5,12)$ with a global retardance factor $d_0 = 10$ mm.

C. Retardance error

Because of the manufacturing tolerance, the thickness of high-order retarders and their retardance may deviate from design values [11]. Therefore, a fabrication tolerance Δd_j of $\pm 5\mu$m was considered and it was assumed that the plates have completely flat and parallel faces. The fabrication tolerance was taken from manufacturers tolerances offered for custom thick birefringent quartz plates.

A global retardance factor of $d_0 = 15$ mm was considered from this test forward, because the lowest total RMS error was obtained with this value (see Table 3). Figure 8 shows the total RMS plots for the extracted Mueller matrix, considering the thickness error from the four retarders. It is observed that the extraction process is sensitive to the thickness error of the first three retarders, and it is about four times less sensitive to the thickness error of the fourth retarder. Immunity is achieved within a fabrication tolerance of up to ± 2 μm for the fourth retarder. This tolerance is much smaller for the first three retarders.

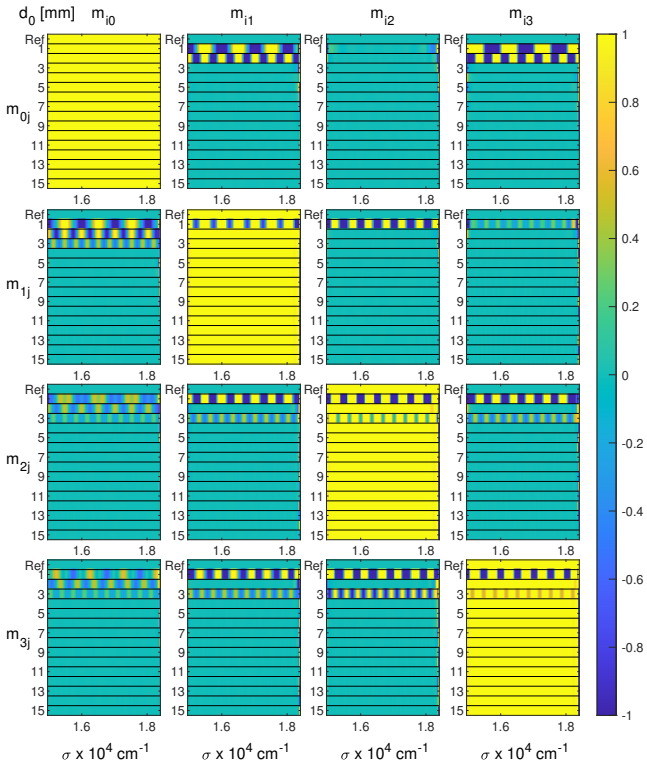

Fig. 6. Normalized Mueller matrix elements (m_{ij}/m_{00}) for d_0 from 1 to 15 mm, with a configuration $(1,2,5,10)$.

D. Alignment error

The assembly process of an instrument is not perfect; therefore, the alignment errors (ϵ_j) of high-order retarders are unavoidable [11]. An alignment tolerance of up to ± 5 degrees was considered for the retarders and the second polarizer.

Figure 9 shows the total RMS plots for the extracted Mueller matrix, considering the alignment error of the four retarders $(\epsilon_1 - \epsilon_4)$ and the second polarizer (ϵ_5). The extraction is acceptable within the tolerance of ± 5 degrees. It is observed that the extraction process is more sensitive to the alignment error on the first retarder, for this retarder immunity is achieved between ± 0.6 degrees. The performance for the other three retarders and the second polarizer is similar, for these elements immunity is achieved within a tolerance of ± 0.8 degrees.

E. Gaussian noise

A random noise distribution was added to the spectrum leaving the MMCS before entering the spectrometer. The amplitudes considered range from 1×10^{-6} to 1, and considering a unit amplitude signal, these values correspond to a range of signal-to-noise ratio (SNR) from 1×10^6 to 1. We also included a reference without noise.

Figure 10 shows the extracted Mueller matrix, considering additive noise. It is easily observed that the MMCS is generally immune to the noise distribution added, except for SNR < 100, see the RMS plots in Fig. 11. However, it can be seen that the sensitivity to the noise is not the same for all the normalized Mueller matrix elements. For example, m_{13}, m_{23}, and m_{32} have a RMS error higher than the immunity condition for the SNR $=$

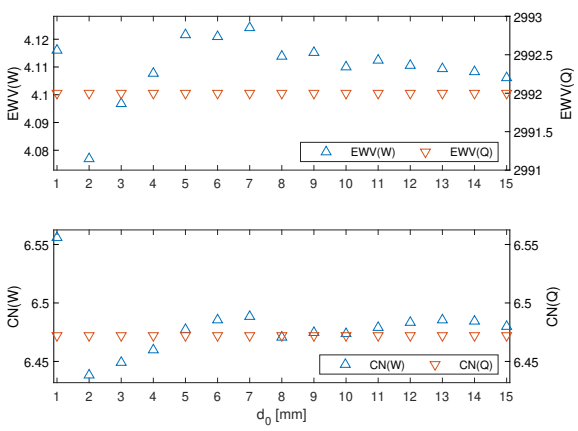

Fig. 7. EWV and CN of the W- and Q-matrix of a MMCS with a $(1,2,5,10)$-configuration against the global retardance factor d_0 from 1 to 15 mm.

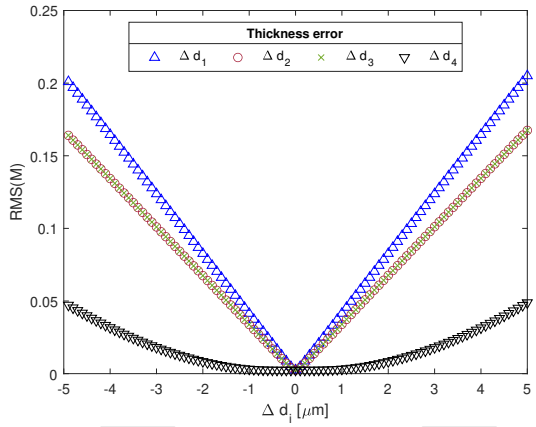

Fig. 8. Total RMS($\mathbf{M}$) error against the thickness error Δd_j of the j-th retarder, for $j = 1,2,3,4$.

1000, whereas, m_{12}, m_{20}, and m_{30} have a total RMS error which is about an order of magnitude smaller for higher SNR levels. This could be important for partial Mueller matrix polarimetry, where optimization is required for the particular Mueller matrix elements to be measured.

4. CONCLUSION

In this paper, the results of analysis and simulations of active channeled polarimeters, specifically with spectral channeling, and including some error sources and measurement noise, were presented. Two figures of merit, equally weighted variance (EWV) and condition number (CN), were studied as metrics of the polarimeter performance and noise immunity. The main metric to evaluate the performance of the polarimeters was the root mean square error (RMS).

Six configurations were compared, three of them are known to have the minimum EWV scores [2], that is the highest immunity to additive noise. Although all six configurations have RMS scores within the immunity condition, it was observed that configurations $(1,2,5,10)$, $(2,1,4,11)$, and $(2,1,5,12)$ offered the lowest RMS scores, between 1×10^{-4} and 1×10^{-5} for most of the unknown sample Mueller matrix elements.

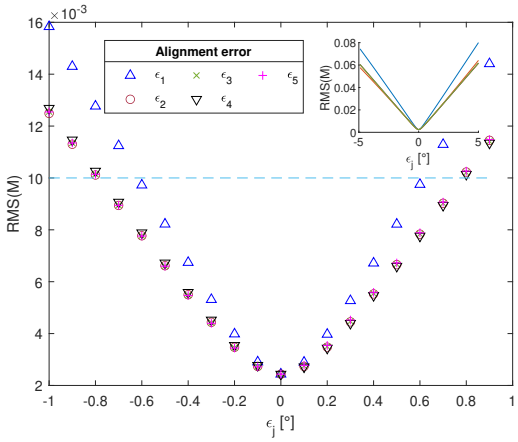

Fig. 9. Total RMS($\mathbf{M}$) error against the alignment error ϵ_j for $j = 1,2,...,5$ (first, second, third, and fourth retarder, and second polarizer, respectively) within a tolerance of ±1 degrees. The nominal orientations of the components are $\theta_1 = 45°, \theta_2 = 0°, \theta_3 = 0°, \theta_4 = 45°$ for the birefringent retarders, and $\theta_5 = 0°$ for the second polarizer.

The MMCS setup analysed together with the particular data extraction algorithm used, requires a global retardance factor ≥ 4 mm in the simulation.

It is also interesting that the errors in axis alignment and retardance value in the thick retarders used in the polarimeter, affect the total RMS error differently, meaning that the error tolerances are different for different retarders. Further studies are being performed to find if this behaviour is general or if it depends on particular polarimeter configurations.

Overall, the extraction of the Mueller matrix elements was achieved with acceptable extraction. We are currently working on further analysis using samples with more complex polarization properties and spectral polarization variations.

Funding. Dirección General de Asuntos del Personal Académico - Universidad Nacional Autónoma de México (PAPIIT-DGAPA, UNAM) (IT100417 and IG100121).

Acknowledgments. Luis Oscar González-Siu acknowledges a grant provided under the Programa Nacional de Posgrados de Calidad (PNPC) of Consejo Nacional de Ciencia y Tecnología (CONACYT) and Programa de Maestría y Doctorado en Ingeniería (PMDI) from the National Autonomous University of Mexico (UNAM).

Disclosures. The authors declare no conflicts of interest.

Data Availability Statement. Data underlying the results presented in this paper are not publicly available at this time but may be obtained from the authors upon reasonable request.

REFERENCES

1. A. S. Alenin and J. S. Tyo, "Task-specific snapshot Mueller matrix channeled spectropolarimeter optimization," in *Polarization: Measurement, Analysis, and Remote Sensing X*, vol. 8364 (2012), pp. 836402–836402–13.
2. A. S. Alenin and J. S. Tyo, "Generalized channeled polarimetry," J. Opt. Soc. Am. A **31**, 1013 (2014).
3. D. E. Aspnes, "Analysis Of Semiconductor Materials And Structures By Spectroellipsometry," in *Spectroscopic Characterization Techniques for Semiconductor Technology III*, vol. 0946 O. J. Glembocki, F. H. Pollak, and F. A. Ponce, eds. (1988), p. 84.

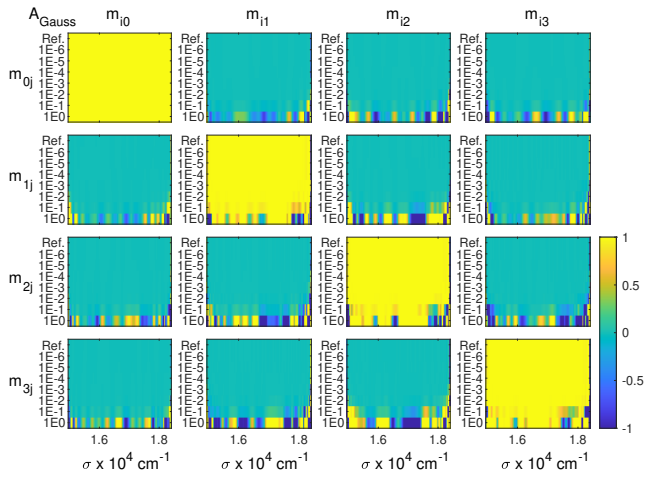

Fig. 10. Normalized Mueller matrix elements (m_{ij}/m_{00}) of the sample (air) with a configuration $(1, 2, 5, 10)$ against the Gaussian noise distribution amplitude.

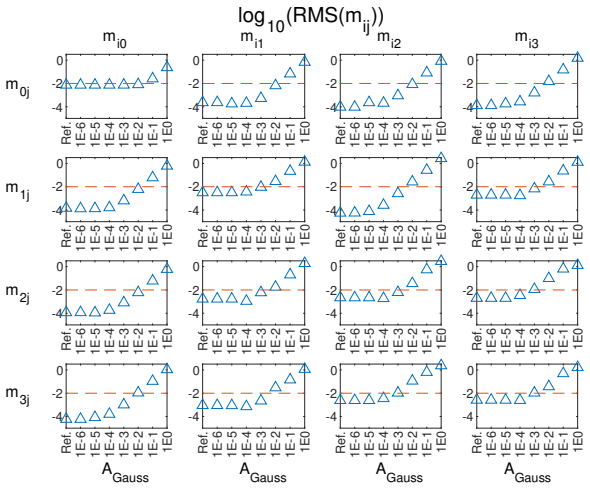

Fig. 11. RMS error of the Mueller matrix elements m_{ij} against the Gaussian noise distribution amplitude.

4. K. Oka and T. Kato, "Spectroscopic polarimetry with a channeled spectrum," Opt. Lett. **24**, 1475 (1999).
5. D. J. Diner, R. A. Chipman, N. A. Beaudry, B. Cairns, L. D. Foo, S. A. Macenka, T. J. Cunningham, S. Seshadri, and C. U. Keller, "An integrated multiangle, multispectral, and polarimetric imaging concept for aerosol remote sensing from space," in *Enabling Sensor and Platform Technologies for Spaceborne Remote Sensing,* vol. 5659 G. J. Komar, J. Wang, and T. Kimura, eds., International Society for Optics and Photonics (SPIE, 2005), p. 88.
6. S. H. Jones, F. J. Iannarilli, C. Hostetler, B. Cairns, A. Cook, J. Hair, D. Harper, Y. Hu, and D. Flittner, "Preliminary airborne measurement results from the Hyperspectral Polarimeter for Aerosol Retrievals (HySPAR)." NASA Earth Sci. Technol. Conf. Proc. pp. 1–6 (2006).
7. N. Gupta and D. R. Suhre, "Acousto-optic tunable filter imaging spectrometer with full Stokes polarimetric capability," Appl. Opt. **46**, 2632 (2007).
8. N. Gupta, "Acousto-optic tunable filter based spectropolarimetric imagers," in *Polarization: Measurement, Analysis, and Remote Sensing VIII,* vol. 6972 D. B. Chenault and D. H. Goldstein, eds., International Society for Optics and Photonics (SPIE, 2008), p. 69720C.
9. B. P. Cumming, G. E. Schröder-Turk, S. Debbarma, and M. Gu, "Bragg-mirror-like circular dichroism in bio-inspired quadruple-gyroid 4srs nanostructures," Light. Sci. & applications **6**, e16192–e16192 (2017).
10. A. Y. Zhu, W. T. Chen, A. Zaidi, Y.-W. Huang, M. Khorasaninejad, V. Sanjeev, C.-W. Qiu, and F. Capasso, "Giant intrinsic chiro-optical activity in planar dielectric nanostructures," Light. Sci. & applications **7**, 17158–17158 (2018).
11. X. Ju, B. Yang, C. Yan, J. Zhang, and W. Xing, "Easily implemented approach for the calibration of alignment and retardation errors in a channeled spectropolarimeter," Appl. Opt. **57**, 8600 (2018).
12. L. Gonzalez-Siu and N. Bruce, "Error Analysis of Channeled Stokes Polarimeters," Appl. Opt. (2021). Doc. ID 423739 (posted 28 April 2021, in press).
13. J. S. Tyo, D. L. Goldstein, D. B. Chenault, and J. A. Shaw, "Review of passive imaging polarimetry for remote sensing applications," Appl. Opt. **45**, 5453 (2006).
14. D. L. Goldstein, *Polarized Light* (CRC Press, New York, 2011), 3rd ed.
15. M. H. Smith, J. B. Woodruff, and J. D. Howe, "<title>Beam wander considerations in imaging polarimetry</title>," in *Polarization: Measurement, Analysis, and Remote Sensing II,* vol. 3754 D. H. Goldstein and D. B. Chenault, eds., International Society for Optics and Photonics (SPIE, 1999), pp. 50–54.
16. K. H. Nordsieck, "A Simple Polarimetric System for the Lick Observatory Image-Tube Scanner," Publ. Astron. Soc. Pac. **86**, 324 (1974).
17. K. Oka, T. Takeda, and Y. Ohtsuka, "Optical Heterodyne Polarimeter for Studying Space-and Time-dependent State of Polarization of Light," J. Mod. Opt. **38**, 1567–1580 (1991).
18. F. J. Iannarilli, Jr., S. H. Jones, H. E. Scott, and P. L. Kebabian, "Polarimetric-spectral intensity modulation (P-SIM): enabling simultaneous hyperspectral and polarimetric imaging," in *Infrared Technology and Applications XXV,* vol. 3698 B. F. Andresen and M. Strojnik, eds., International Society for Optics and Photonics (SPIE, 1999), p. 474.
19. N. Hagen, "Calibration methods for snapshot Mueller matrix spectropolarimetry," in *Optical Technology and Measurement for Industrial Applications 2020,* vol. 1152302 T. Hatsuzawa, R. Tutsch, and T. Yoshizawa, eds. (SPIE, Yokohama, 2020), p. 10.
20. R. A. Chipman, "Polarimetric impulse response and polarimetric transfer function for time-sequential polarimeters," in *Polarimetry: Radar, Infrared, Visible, Ultraviolet, and X-Ray,* vol. 1317 R. A. Chipman and J. W. Morris, eds. (1990), pp. 223–241.
21. N. Hagen, K. Oka, and E. L. Dereniak, "Snapshot Mueller matrix spectropolarimeter: erratum," Opt. Lett. **38**, 1675 (2013).
22. G. Ghosh, "Dispersion-equation coefficients for the refractive index and birefringence of calcite and quartz crystals," Opt. Commun. **163**, 95–102 (1999).
23. D. S. Sabatke, A. M. Locke, E. L. Dereniak, and R. W. McMillan, "Linear calibration and reconstruction techniques for channeled spectropolarimetry," Opt. Express **11**, 2940 (2003).
24. M. Takeda, H. Ina, and S. Kobayashi, "Fourier-transform method of fringe-pattern analysis for computer-based topography and interferometry," J. Opt. Soc. Am. **72**, 156 (1982).
25. F. Harris, "On the use of windows for harmonic analysis with the discrete Fourier transform," Proc. IEEE **66**, 51–83 (1978).
26. D. S. Sabatke, M. R. Descour, E. L. Dereniak, W. C. Sweatt, S. A. Kemme, and G. S. Phipps, "Optimization of retardance for a complete Stokes polarimeter," Opt. Lett. **25**, 802 (2000).
27. T. Mu, Z. Chen, C. Zhang, and R. Liang, "Optimal configurations of full-Stokes polarimeter with immunity to both Poisson and Gaussian noise," J. Opt. **18**, 055702 (2016).
28. R. M. A. Azzam, "Photopolarimetric measurement of the Mueller matrix by Fourier analysis of a single detected signal," Opt. Lett. **2**, 148 (1978).